

Light curve and spectral evolution of the Type IIb SN 2011fu

Brajesh Kumar^{1,2} *, S. B. Pandey¹, D. K. Sahu³, J. Vinko⁴,
 A. S. Moskvitin⁵, G. C. Anupama³, V. K. Bhatt¹, A. Ordasi⁶,
 A. Nagy⁴, V. V. Sokolov⁵, T. N. Sokolova⁵, V. N. Komarova⁵,
 Brijesh Kumar¹, Subhash Bose¹, Rupak Roy¹, Ram Sagar¹

¹*Aryabhata Research Institute of observational sciencES, Manora Peak, Nainital 263129, India*

²*Institut d’Astrophysique et de Géophysique, Université de Liège, Allée du 6 Août 17, Bât B5c, 4000 Liège, Belgium*

³*Indian Institute of Astrophysics, Koramangala, Bangalore 560 034, India*

⁴*Department of Optics & Quantum Electronics, University of Szeged, Dóm tér 9, Szeged, Hungary*

⁵*Special Astrophysical Observatory, Nizhnij Arkhyz, Karachaevo-Cherkesia, 369167 Russia*

⁶*Department of Experimental Physics, University of Szeged, Dóm tér 9, Szeged, Hungary*

Accepted ———, Received ———; in original form ———

ABSTRACT

We present the low-resolution spectroscopic and *UBVRI* broad-band photometric investigations of the Type IIb supernova 2011fu, discovered in UGC 01626. The photometric follow-up of this event has been initiated a few days after the explosion and covers a period of about 175 days. The early-phase light curve shows a rise followed by steep decay in all bands and shares properties very similar to that seen in case of SN 1993J, with a possible detection of the adiabatic cooling phase. Modelling of the quasi-bolometric light curve suggests that the progenitor had an extended ($\sim 1 \times 10^{13}$ cm), low-mass ($\sim 0.1 M_{\odot}$) H-rich envelope on top of a dense, compact ($\sim 2 \times 10^{11}$ cm), more massive ($\sim 1.1 M_{\odot}$) He-rich core. The nickel mass synthesized during the explosion was found to be $\sim 0.21 M_{\odot}$, slightly larger than seen in case of other Type IIb SNe. The spectral modelling performed with *SNOW* suggests that the early-phase line velocities for H and Fe II features were $\sim 16000 \text{ km s}^{-1}$ and $\sim 14000 \text{ km s}^{-1}$, respectively. Then the velocities declined up to day +40 and became nearly constant at later epochs.

Key words: Supernovae: general - supernovae: individual (SN2011fu)

1 INTRODUCTION

It is commonly recognized that core-collapse supernovae (CCSNe) represent the final stages of the life of massive stars ($M > 8\text{--}10 M_{\odot}$) (Heger et al., 2003; Anderson & James, 2009; Smartt, 2009). Generally, the fate of massive stars is governed by its mass, metallicity, rotation and magnetic field (Fryer, 1999; Heger et al., 2003; Woosley & Janka, 2005). Massive stars show a wide variety in these fundamental parameters, causing diverse observational properties among various types of CCSNe. The presence of dominant hydrogen lines in the spectra of Type II SNe strongly suggests that their progenitors belong to massive stars which are still surrounded by significantly thick hydrogen envelope before

the explosion (see Filippenko, 1997, for a review on different types of SNe). On the contrary, Type Ib events are H-deficient but He is still present in their spectra, unlike to Type Ic SNe, where both H and He features are absent. After the discovery of SN 1987K, another class, termed as Type IIb (see Filippenko, 1988; Woosley et al., 1987), was included in the CCSN zoo, and the observational properties of these SNe closely resemble those of Type II SNe during the early phases, while they are more similar to Type Ib/c events at later epochs.

However, in a few cases, the spectral classification of Type IIb SNe is more controversial: for example, SN 2000H (Benetti et al., 2000; Branch et al., 2002; Elmhamdi et al., 2006); SN 2003bg (Filippenko & Chornock, 2003; Soderberg et al., 2006); SN 2007Y (although this event is classified as Type Ib/c by e.g. Monard (2007);

* E-mail: brajesh@aries.res.in, brajesharies@gmail.com

Stritzinger et al. (2009) however, Maurer et al. (2010) suggested that it is a Type IIb) and SN 2009mg (Prieto, 2009; Roming et al., 2009a; Stritzinger, 2010)). SNe of Type IIb are further divided into two subgroups: Type cIIb with compact progenitors like SNe 1996cb, 2001lig and 2008ax, and Type eIIb with extended progenitors, e.g SNe 1993J and 2001gd (Chevalier & Soderberg, 2010).

Type IIb and Type Ib/c SNe are collectively known as “stripped envelope” CCSNe (Clochiatti et al., 1997) as the outer envelopes of hydrogen and/or helium of their progenitors are partially or completely removed before the explosion. The possible physical mechanisms behind this process may be stellar winds (Puls et al., 2008) or interaction with a companion star in a binary system where mass transfer occurs due to Roche lobe overflow (Podsiadlowski et al., 1992). There are several studies about the discovery of the progenitors of Type IIb SNe but the debate about how they manage to keep only a thin layer of hydrogen, is still on (Aldering et al., 1994; Maund et al., 2004; Ryder et al., 2006; Crockett et al., 2008; Sonbas et al., 2008; Arcavi et al., 2011; Maund et al., 2011; Van Dyk et al., 2011; Soderberg et al., 2012).

To date, approximately 77¹ Type IIb SNe are known, but only a few of them have been properly monitored and well-studied. Among them, SNe 1987K (Filippenko, 1988); 1993J (Schmidt et al., 1993; Lewis et al., 1994; Richmond et al., 1994); 1996cb (Qiu et al., 1999), 2003bg (Hamuy et al., 2009; Mazzali et al., 2009); 2008ax (Pastorello et al., 2008; Roming et al., 2009b; Chornock et al., 2011; Taubenberger et al., 2011); 2009mg (Oates et al., 2012); 2011ei (Milisavljevic et al., 2012) and more recently 2011dh (Arcavi et al., 2011; Martí-Vidal et al., 2011; Maund et al., 2011; Van Dyk et al., 2011; Bersten et al., 2012; Bietenholz et al., 2012; Horesh et al., 2012; Krauss et al., 2012; Soderberg et al., 2012; Vinkó et al., 2012) were remarkably well-studied.

An interesting property of the observed light curves (LCs) of a few Type IIb SNe is the initial peak and rapid decline followed by a subsequent rise and a secondary maximum. The first peak is thought to be due to the break-out of the SN shock from the extended progenitor envelope (Falk & Arnett, 1977). The properties of the shock break-out peak depend on the envelope mass and the density structure of the outer layers. The shock break-out phase can last from seconds to days. Therefore, early discovery and rapid-cadence early-time observations may help in understanding the properties of the outer envelope of massive stars in a better way (Gal-Yam et al., 2011).

In this paper, we present the results from photometric and spectroscopic monitoring of SN 2011fu starting shortly after the discovery and extending up to nebular phases. The photometric and spectroscopic properties of this event reveal that SN 2011fu is a Type IIb supernova. The type determination for this SN was verified with SNID (Blondin & Tonry, 2007), highlighting an excellent resemblance of the object with SN 1993J.

The paper is organized as follows. The photometric and

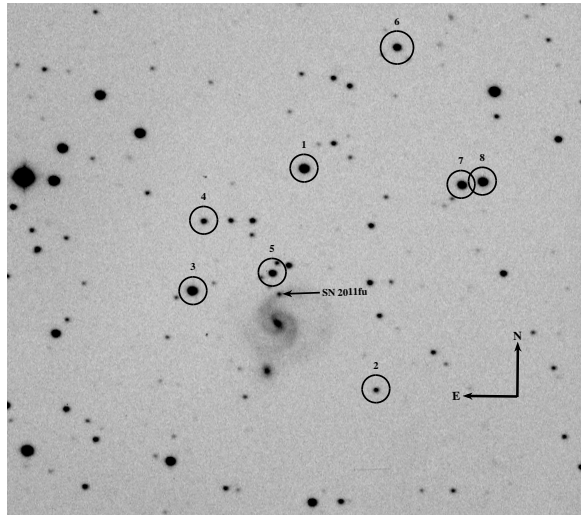


Figure 1. The V-band image of the SN 2011fu field around the galaxy UGC 01626, observed on 2011 November 16 with the 1-m ST, India. The SN is marked with a black arrow. The reference standard stars used for calibration are marked with numbers 1-8. On this image, north is up and east is to the left.

spectroscopic observations are presented in Section 2, where the methods for data reduction and analysis are described. In Section 3, we analyze the light and colour curves. In Sections 4, we describe and model the bolometric LC. Section 5 deals with the spectroscopic modelling using the SYNOW code. In Section 6, we discuss the metallicities of the host galaxy of SN 2011fu along with those of other CCSNe. Finally, the results are summarized in Section 7.

2 OBSERVATIONS AND DATA ANALYSIS

SN 2011fu was discovered in a spiral arm of the galaxy UGC 01626 (type SAB(rs)c) by F. Ciabattari and E. Mazzoni (Ciabattari et al., 2011) on 2011 September 21.04 (UT) with a 0.5-m Newtonian telescope in the course of the Italian Supernovae Search Project. The brightness of the SN at the time of discovery was reported to be at mag ~ 16 (unfiltered). It was located 2'' west and 26'' north of the center of the host galaxy, with coordinates $\alpha = 02^{\text{h}}08^{\text{m}}21^{\text{s}}.41$, $\delta = +41^{\circ}29'12''.3$ (equinox 2000.0) (Ciabattari et al., 2011). The host galaxy has a heliocentric velocity and redshift of $5543 \pm 11 \text{ km s}^{-1}$ and $z = 0.018489 \pm 0.000037^2$, respectively. The first spectrum of SN2011fu was obtained on 2011 September 23.84 UT with the Ekar-Copernico 1.82-m telescope (range 360-810 nm; resolution 2.2 nm) by Tomasella et al. (2011), showing a blue continuum with superimposed weak H and HeI 587.6-nm features, which led to the classification as a young Type II SN.

2.1 Optical Photometry

The prompt photometric follow-up of SN 2011fu started shortly after the discovery and continued using three

¹ <http://heasarc.gsfc.nasa.gov/W3Browse/star-catalog/asiagosn.html>

² HyperLEDA - <http://leda.univ-lyon1.fr>

ground-based telescopes in India. The majority of the observations were made using the 2-m *Himalayan Chandra Telescope* (HCT) of the Indian Astronomical Observatory, Hanle and the 1-m *Sampurnanand Telescope* (ST) at the Aryabhata Research Institute of observational sciences (ARIES), Nainital, India. All observations were performed in Bessell *UBVRI* bands.

The HCT photometric observations started on 2011 September 28 using the Himalaya Faint Object Spectrograph Camera (HFOSC). The central $2k \times 2k$ region of a $2k \times 4k$ SITE CCD chip was used for imaging which provided an image scale of $0.296 \text{ arcsec pixel}^{-1}$ across a $10 \times 10 \text{ arcmin}^2$ field-of-view.

Further photometric observations were carried out using a $2k \times 2k$ CCD camera at the $f/13$ Cassegrain focus of the 1-m ST telescope situated at ARIES, Nainital. The CCD chip has square pixels of $24 \times 24 \mu\text{m}$, a scale of $0.38 \text{ arcsec per pixel}$ and the entire chip covers a field of $13 \times 13 \text{ arcmin}^2$ on the sky. The gain and readout noise of the CCD camera are 10 electron per ADU and 5.3 electrons, respectively. A finding chart showing the field of the SN 2011fu along with the local standard stars is presented in Fig. 1.

In addition, we also observed this SN in *V* and *R* bands on 2011 December 01 and 2012 March 02 using the 1.3m telescope DFOT³ (Sagar et al., 2011, 2012), recently installed at Devasthal, Nainital.

To improve the signal-to-noise ratio (S/N), all the photometric observations were carried out with 2×2 binning. Along with science frames several bias and twilight flat frames were also collected. Alignment and determination of mean FWHM on all science frames were performed after the usual bias subtraction, flat fielding and cosmic-ray removal. The standard tasks available in IRAF⁴ and DAOPHOT⁵ (Stetson, 1987, 1992) were used for pre-processing and photometry.

The pre-processing steps for images taken with all three telescopes were performed in a similar fashion. The stellar FWHM on the *V*-band frames typically varied from $2''$ to $4''$, with a median value of around $2''.5$. We also co-added individual frames, wherever necessary, before computing the final photometry.

For photometric calibration, we observed the standard field PG0231 (Landolt, 2009) in *UBVRI* bands with the 1-m ST on 2011 December 17 under good photometric conditions (transparent sky, seeing FWHM in *V* $\sim 2''$). The profile fitting technique was applied for the photometry of SN 2011fu

and Landolt field and then instrumental magnitudes were converted into standard system following least-square linear regression procedures outlined in Stetson (1992). Atmospheric extinction values (0.57, 0.28, 0.17, 0.11 and 0.07 mag per unit airmass for *U*, *B*, *V*, *R* and *I* bands, respectively) for the site were adopted from Kumar et al. (2000). The chosen Landolt stars for calibration had the brightness range of $12.77 \leq V \leq 16.11$ mag and colour range of $-0.33 \leq B - V \leq 1.45$ mag. Using these stars, transformation to the standard system was derived by applying the following zero-points and colour coefficients:

$$u - U = (7.27 \pm 0.01) + (-0.08 \pm 0.02)(U - B)$$

$$b - B = (4.90 \pm 0.004) + (-0.04 \pm 0.01)(B - V)$$

$$v - V = (4.34 \pm 0.01) + (-0.04 \pm 0.01)(B - V)$$

$$r - R = (4.19 \pm 0.01) + (-0.04 \pm 0.01)(V - R)$$

$$i - I = (4.60 \pm 0.02) + (0.04 \pm 0.02)(V - I)$$

Here *U*, *B*, *V*, *R*, *I* are the catalogue magnitudes and *u*, *b*, *v*, *r*, *i* are the corresponding instrumental magnitudes. Table 1 lists the coordinates and magnitudes of the eight local secondary standard stars in the SN field.

To estimate the possible contribution from the host galaxy to the measured supernova fluxes, we used the *ISIS*⁶ image subtraction package. We acquired deep images (having total exposure times of more than 20 minutes) in *BVRI* bands with the HCT telescope on 25 August 2012 under good sky conditions. As the supernova was not detected in anyone of these frames, we used them as template frames for image subtraction. We found minor differences, not exceeding 0.1 mag, between the SN magnitudes with and without applying the image subtraction for the data at later epochs i.e. 70 days after the first observation. The final results of our SN photometry (without applying image subtraction corrections) along with robustly determined PSF errors, are presented in Table 2.

2.2 Spectroscopy

Spectroscopic observations of SN 2011fu were obtained at 8 epochs, between 2011 September 28 (JD 2455833.27) and December 22 (JD 2455918.11). A journal of these observations is given in Table 3. The SN spectra were taken with the HFOSC instrument mounted at the 2-m Himalayan Chandra Telescope. All spectra were obtained using grisms Gr#7 (wavelength range 3500 - 7800 Å) and Gr#8 (wavelength range 5200 - 9200 Å). FeAr and FeNe arc lamp spectra were applied for wavelength calibration. Spectrophotometric standard were also observed with a broader slit to correct for the instrumental response and flux calibration.

The reduction of the spectroscopic data were carried out in a standard manner using various tasks available within IRAF. First, all images were bias-subtracted and flat fielded. Then, one dimensional spectra were extracted from the two-dimensional cleaned images using the optimal extraction algorithm (Horne, 1986). The wavelength calibration was computed using the arc spectra mentioned above. The accuracy of the wavelength calibration was checked using the

³ DFOT uses 2048×2048 ANDOR CCD camera having $13.5 \times 13.5 \mu\text{m}$ pixels mounted at the $f/4$ Cassegrain focus of the telescope. With $0.54 \text{ arcsec per pixel}$ plate scale, the entire chip covers a $18 \times 18 \text{ arcmin}^2$ field-of-view on the sky. The CCD can be read out with 31, 62, 500 and 1000 kHz speed, with system RMS noise of 2.5, 4.1, 6.5, 7 electrons and gain of 0.7, 1.4, 2, 2 electron/ADU respectively. We selected the 500 kHz readout frequency during our observations.

⁴ IRAF stands for Image Reduction and Analysis Facility distributed by the National Optical Astronomy Observatories which is operated by the Association of Universities for research in Astronomy, Inc. under co-operative agreement with the National Science Foundation.

⁵ DAOPHOT stands for Dominion Astrophysical Observatory Photometry.

⁶ <http://www2.iap.fr/users/alard/package.html>

Table 1. Identification number (ID), coordinates (α, δ) and calibrated magnitudes of standard stars in the field of SN 2011fu.

Star ID	α_{J2000} (h m s)	δ_{J2000} ($^{\circ}$ $'$ $''$)	U (mag)	B (mag)	V (mag)	R (mag)	I (mag)
1	02 08 19.66	+41 30 53.4	15.59 \pm 0.02	15.47 \pm 0.02	14.80 \pm 0.01	14.38 \pm 0.02	14.03 \pm 0.02
2	02 08 14.25	+41 27 51.8	18.39 \pm 0.09	18.17 \pm 0.02	17.59 \pm 0.02	17.16 \pm 0.02	16.83 \pm 0.03
3	02 08 27.70	+41 29 11.4	16.29 \pm 0.02	15.70 \pm 0.02	14.86 \pm 0.02	14.34 \pm 0.02	13.93 \pm 0.03
4	02 08 26.92	+41 30 07.5	17.53 \pm 0.04	17.58 \pm 0.02	17.07 \pm 0.02	16.70 \pm 0.02	16.40 \pm 0.03
5	02 08 21.94	+41 29 26.9	16.78 \pm 0.03	16.77 \pm 0.02	16.21 \pm 0.01	15.84 \pm 0.02	15.54 \pm 0.02
6	02 08 12.72	+41 32 34.8	16.36 \pm 0.02	16.45 \pm 0.02	15.85 \pm 0.01	15.44 \pm 0.02	15.07 \pm 0.02
7	02 08 08.04	+41 30 41.3	16.32 \pm 0.02	16.07 \pm 0.02	15.38 \pm 0.01	14.97 \pm 0.02	14.61 \pm 0.02
8	02 08 06.54	+41 30 43.7	17.23 \pm 0.03	16.03 \pm 0.02	14.93 \pm 0.02	14.32 \pm 0.02	13.78 \pm 0.02

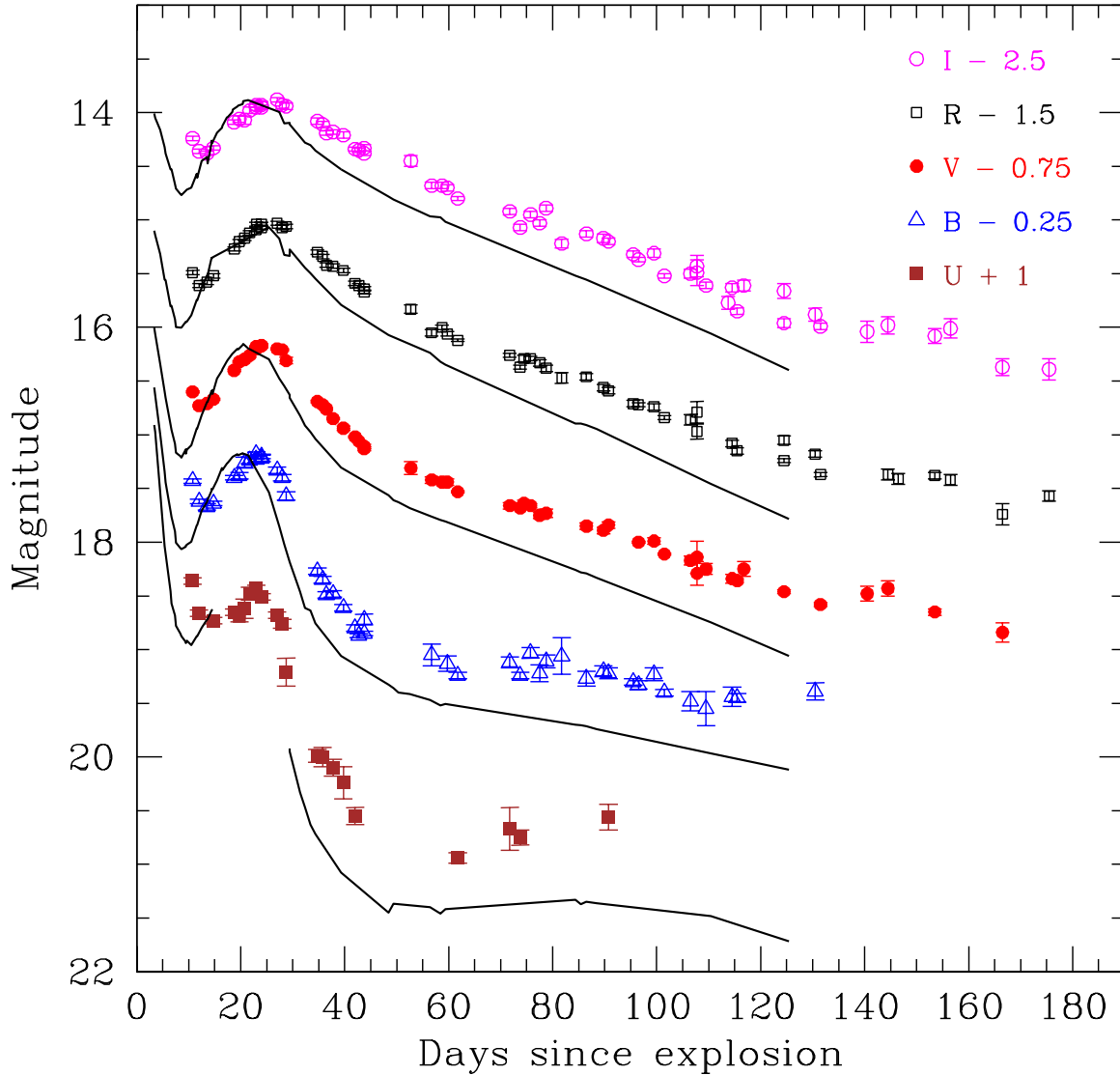
**Figure 2.** Observed *UBVR* light curves of SN 2011fu. For clarity, the light curves in different bands have been shifted vertically by the values indicated in the legend. Black solid lines represent the light curves of SN 1993J over-plotted with appropriate shifts. The explosion date of SN 2011fu was taken to be 2011 September 18 ± 2 , as described in subsection 3.1.

Table 2. Photometric observational log of SN 2011fu

JD	Phase ^a (Days)	<i>U</i> (mag)	<i>B</i> (mag)	<i>V</i> (mag)	<i>R</i> (mag)	<i>I</i> (mag)	Telescope
2455833.23	+10.73	17.36± 0.03	17.68 ± 0.02	17.35± 0.01	16.99 ± 0.02	16.74 ± 0.02	HCT
2455834.49	+11.99	17.66± 0.03	17.87 ± 0.02	17.48± 0.01	17.11 ± 0.02	16.86 ± 0.02	HCT
2455836.15	+13.65	–	17.92 ± 0.03	17.46± 0.01	17.08 ± 0.02	16.88 ± 0.02	HCT
2455837.26	+14.76	17.73± 0.03	17.89 ± 0.02	17.42± 0.01	17.02 ± 0.02	16.83 ± 0.02	HCT
2455841.23	+18.73	17.65± 0.03	17.65 ± 0.02	17.15± 0.01	16.77 ± 0.02	16.59 ± 0.02	ST
2455842.30	+19.80	17.69± 0.05	17.63 ± 0.03	17.07± 0.01	16.70 ± 0.02	16.56 ± 0.03	ST
2455843.27	+20.77	17.62± 0.09	17.51 ± 0.05	17.05± 0.02	16.67 ± 0.02	16.57 ± 0.04	ST
2455844.21	+21.71	17.48± 0.06	17.49 ± 0.03	17.01± 0.02	16.62 ± 0.02	16.48 ± 0.03	ST
2455845.44	+22.94	17.43± 0.03	17.48 ± 0.03	16.95± 0.02	16.59 ± 0.02	16.45 ± 0.03	ST
2455845.43	+22.93	–	17.43 ± 0.02	16.93± 0.01	16.54 ± 0.02	16.43 ± 0.02	HCT
2455846.44	+23.94	17.51± 0.03	17.47 ± 0.03	16.92± 0.02	16.57 ± 0.02	16.43 ± 0.03	ST
2455846.43	+23.93	–	17.45 ± 0.02	16.92± 0.01	16.54 ± 0.02	16.45 ± 0.02	HCT
2455849.41	+26.91	17.68± 0.03	17.58 ± 0.03	16.95± 0.01	16.53 ± 0.02	16.38 ± 0.02	HCT
2455850.40	+27.89	17.76± 0.04	17.65 ± 0.03	16.96± 0.01	16.57 ± 0.02	16.43 ± 0.03	HCT
2455851.31	+28.81	18.21± 0.13	17.82 ± 0.04	17.06± 0.03	16.56 ± 0.02	16.44 ± 0.03	ST
2455857.30	+34.80	18.99± 0.06	18.52 ± 0.03	17.44± 0.01	16.80 ± 0.02	16.58 ± 0.03	ST
2455858.32	+35.82	19.00± 0.09	18.60 ± 0.03	17.47± 0.01	16.84 ± 0.02	16.61 ± 0.03	ST
2455859.18	+36.68	–	18.74 ± 0.03	17.51± 0.01	16.92 ± 0.02	16.69 ± 0.02	HCT
2455860.30	+37.80	19.10± 0.08	18.73 ± 0.03	17.60± 0.01	16.93 ± 0.02	16.68 ± 0.02	ST
2455862.30	+39.80	19.24± 0.15	18.86 ± 0.03	17.69± 0.02	16.97 ± 0.02	16.71 ± 0.03	ST
2455864.40	+41.90	19.55± 0.08	19.05 ± 0.03	17.77± 0.01	17.09 ± 0.02	16.84 ± 0.02	HCT
2455865.35	+42.85	–	19.12 ± 0.02	17.81± 0.01	17.11 ± 0.02	16.85 ± 0.02	HCT
2455866.23	+43.73	–	18.97 ± 0.05	17.88± 0.02	17.14 ± 0.02	16.83 ± 0.03	ST
2455866.26	+43.76	–	19.10 ± 0.02	17.86± 0.02	17.17 ± 0.02	16.88 ± 0.02	HCT
2455875.22	+52.72	–	–	18.06± 0.06	17.33 ± 0.04	16.95 ± 0.05	ST
2455879.28	+56.78	–	19.30 ± 0.10	18.17± 0.03	17.55 ± 0.03	17.18 ± 0.03	ST
2455881.26	+58.76	–	–	18.19± 0.02	17.50 ± 0.02	17.18 ± 0.03	HCT
2455882.33	+59.83	–	19.38 ± 0.07	18.19± 0.03	17.56 ± 0.02	17.20 ± 0.03	ST
2455884.27	+61.78	19.94± 0.05	19.49 ± 0.03	18.28± 0.01	17.62 ± 0.01	17.30 ± 0.02	HCT
2455894.23	+71.73	19.67± 0.20	19.37 ± 0.05	18.41± 0.03	17.76 ± 0.02	17.42 ± 0.03	ST
2455896.28	+73.78	19.75± 0.07	19.49 ± 0.03	18.43± 0.01	17.87 ± 0.02	17.57 ± 0.03	HCT
2455897.08	+74.58	–	–	18.39± 0.03	17.79 ± 0.03	–	DFOT
2455898.30	+75.80	–	19.28 ± 0.05	18.41± 0.02	17.79 ± 0.02	17.45 ± 0.03	ST
2455900.17	+77.66	–	19.47 ± 0.08	18.50± 0.03	17.83 ± 0.03	17.53 ± 0.03	ST
2455901.24	+78.74	–	19.36 ± 0.06	18.48± 0.04	17.88 ± 0.03	17.39 ± 0.03	ST
2455904.28	+81.78	–	19.31 ± 0.17	–	17.97 ± 0.05	17.72 ± 0.04	HCT
2455909.18	+86.68	–	19.52 ± 0.07	18.60± 0.03	17.96 ± 0.03	17.63 ± 0.03	ST
2455912.28	+89.78	–	19.45 ± 0.05	18.64± 0.03	18.06 ± 0.03	17.67 ± 0.04	ST
2455913.24	+90.73	19.56± 0.12	19.47 ± 0.05	18.59± 0.03	18.09 ± 0.03	17.70 ± 0.03	ST
2455918.18	+95.68	–	19.55 ± 0.03	–	18.21 ± 0.03	17.82 ± 0.03	HCT
2455919.11	+96.61	–	19.58 ± 0.04	18.75± 0.01	18.22 ± 0.02	17.87 ± 0.02	HCT
2455922.17	+99.67	–	19.48 ± 0.06	18.74± 0.03	18.24 ± 0.03	17.81 ± 0.04	ST
2455924.10	+101.60	–	19.65 ± 0.03	18.86± 0.01	18.34 ± 0.02	18.02 ± 0.02	HCT
2455929.17	+106.67	–	19.73 ± 0.09	18.92± 0.04	18.36 ± 0.05	18.00 ± 0.04	ST
2455930.27	+107.76	–	–	19.04± 0.11	18.47 ± 0.07	17.99 ± 0.12	ST
2455930.27	+108.73	–	–	18.89± 0.15	18.29 ± 0.10	17.93 ± 0.10	ST
2455932.15	+109.65	–	19.80 0.16	19.00± 0.05	–	18.11 ± 0.03	HCT
2455936.25	+113.75	–	–	–	–	18.27 ± 0.06	HCT
2455937.16	+114.66	–	19.69 ± 0.09	19.09± 0.04	18.58 ± 0.03	18.13 ± 0.04	HCT
2455938.08	+115.58	–	19.70 ± 0.04	19.11± 0.02	18.65 ± 0.03	18.35 ± 0.03	HCT
2455939.23	+116.73	–	–	19.00± 0.07	–	18.11 ± 0.05	ST
2455947.06	+124.56	–	–	19.21± 0.02	18.74 ± 0.02	18.46 ± 0.04	HCT
2455947.16	+124.66	–	–	–	18.55 ± 0.04	18.16 ± 0.07	ST
2455953.08	+130.58	–	19.64 ± 0.08	–	18.68 ± 0.03	18.38 ± 0.06	ST
2455954.16	+131.66	–	–	19.33± 0.02	18.87 ± 0.02	18.49 ± 0.03	HCT
2455963.14	+140.64	–	–	19.23± 0.07	–	18.54 ± 0.10	ST
2455967.11	+144.61	–	–	19.18± 0.07	18.87 ± 0.05	18.48 ± 0.08	ST
2455969.09	+146.59	–	–	–	18.91 ± 0.05	–	ST
2455976.07	+153.56	–	–	19.40± 0.03	18.88 ± 0.03	18.58 ± 0.07	ST
2455979.12	+156.62	–	–	–	18.92 ± 0.05	18.51 ± 0.09	ST
2455989.08	+166.58	–	–	19.59± 0.09	19.24 ± 0.10	18.87 ± 0.08	DFOT, ST
2455998.08	+175.58	–	–	–	19.07 ± 0.05	18.89 ± 0.10	ST
2456159.34	+336.84	–	>22.5	>22	>21.5	>21	HCT

Table 3. Log of spectroscopic observations of SN 2011fu.

Date	J.D.	Phase ^a (Days)	Range (Å)	Resolution (Å)
2011-09-28	2455833.28	+10.78	3500-7800; 5200-9250	7
2011-09-29	2455834.41	+11.92	3500-7800; 5200-9250	7
2011-10-01	2455836.23	+13.73	3500-7800; 5200-9250	7
2011-10-14	2455849.43	+26.93	3500-7800; 5200-9250	7
2011-10-29	2455864.41	+41.91	3500-7800; 5200-9250	7
2011-10-31	2455866.36	+43.86	3500-7800; 5200-9250	7
2011-11-23	2455889.15	+66.65	3500-7800; 5200-9250	7
2011-12-22	2455918.11	+95.61	3500-7800	7

^a with reference to the explosion epoch JD 2455822.5

night sky emission lines and small shifts were applied to the observed spectra whenever required. The instrumental response curves were determined using the spectrophotometric standards observed on the same night as the SN, and the SN spectra were calibrated to a relative flux scale. When the spectrophotometric standards could not be observed, the response curve based on observations in a night close in time to the SN observation was adopted. The flux calibrated spectra in the two regions were combined to a weighted mean to obtain the final spectrum on a relative flux scale.

Finally, the spectra were brought to an absolute flux scale using zero points determined from the calibrated, broad-band *UBVRI* magnitudes. The SN spectra were also corrected for the redshift of the host galaxy ($z = 0.018$), and de-reddened assuming a total reddening of $E(B - V) = 0.22$ mag (see Sub-section 3.3). The telluric lines have not been removed from the spectra.

3 LIGHT CURVES OF SN 2011FU

In this section, we present the multi-band light curves of SN 2011fu and their comparison with SN 1993J light curves and their temporal properties. A brief discussion about the explosion epoch of SN 2011fu is presented in the following sub-section.

3.1 Explosion epoch of SN 2011fu

The detection of very early time light curve features of SN 2011fu, similar to that seen in case of SN 1993J, indicates a very young age at the time of discovery. Very sharp rise followed by a relatively fast decline are explained as the detection of cooling phase and depends mainly on the ^{56}Ni mixing and the progenitor radius, as shown by hydrodynamical models of H-stripped CCSNe (Shigeyama et al., 1994; Woosley et al., 1994; Blinnikov et al., 1998; Bersten et al., 2012). For example, in the case of SN 2011dh, for progenitor radius of $< 300 R_{\odot}$, the cooling phase ends at ~ 5 days after the explosion (see Figure-10 of Bersten et al., 2012).

In the literature, the first detection of SN 2011fu has been reported to be 2011 September 20.708 (Z. Jin and X. Gao, Mt. Nanshan, China). However, according to Ciabattari et al. (2011), this object was not visible on 2011 August 10 at SN location, putting a stringent limit to the explosion date. We collected following pieces of evidences to put a constrain on the explosion date of SN 2011fu.

(i) For CCSNe of Type Ib and IIb, the explosion dates have been estimated to be ~ 20 days prior to the *V*-band maxima (Richardson et al., 2006; Drout et al., 2011) (see also Milisavljevic et al., 2012).

(ii) Type IIb SNe also exhibit bluer $B - V$ colour ~ 40 days after the explosion (Pastorello et al., 2008), giving an indication about the explosion epoch.

(iii) The SNID (Blondin & Tonry, 2007) fitting on initial four spectra of SN 2011fu indicates that explosion of this event would have occurred around 2011 September 20. However, SNID fit for the later three epochs of spectra (after *V* band maximum) gives rise to 2011 September 17 as the explosion date.

(iv) In some of the well studied type IIb SNe, the explosion epoch is better constrained (e.g SN 1993J, SN 2008ax and SN 2011dh) and their early light curve features indicate that the adiabatic cooling phase may be observable for several days after the explosion and this duration depends upon the volume of the photospheric shell (Romig et al., 2009b), as determined in case of SN 1993J (Wheeler et al., 1993; Lewis et al., 1994; Barbon et al., 1995), SN 2008ax (Romig et al., 2009b) and SN 2011dh (Arcavi et al., 2011).

Based on above evidences, we have adopted 2011 September 18 ± 2 as the explosion epoch for SN 2011fu and it will be used for the further discussions in this article.

3.2 Light curve analysis

In Fig. 2, we plot the calibrated *UBVRI* light curves of SN 2011fu. The LCs span ~ 175 days after the explosion. It is clear from Fig. 2 that the photometric observations of this supernova started shortly after explosion, showing the early declining phase in all bands, which is possibly related to the cooling tail after the shock break-out from an extended progenitor envelope (Chevalier, 1992; Waxman et al., 2007; Chevalier & Fransson, 2008; Nakar & Sari, 2010). The LCs of SN 2011fu are strikingly similar to those of SN 1993J, both in the initial and the following phases, exhibiting valley-like structures followed by rising peaks in all bands. At late epochs the LCs are monotonically decreasing in all bands, as expected for expanding, cooling ejecta heated by only the radioactive decay of ^{56}Ni and ^{56}Co .

Beside SNe 1993J and 2011dh, SN 2011fu is the third known case among IIb SNe to date where all the initial decline phase, the rise of the broader secondary peak and the final decline have been observed (although Romig et al.

Table 4. Epochs of the LC valley (t_v) and the secondary peak (t_p) in days after explosion, and their respective apparent magnitudes for SN 2011fu and SN 1993J.

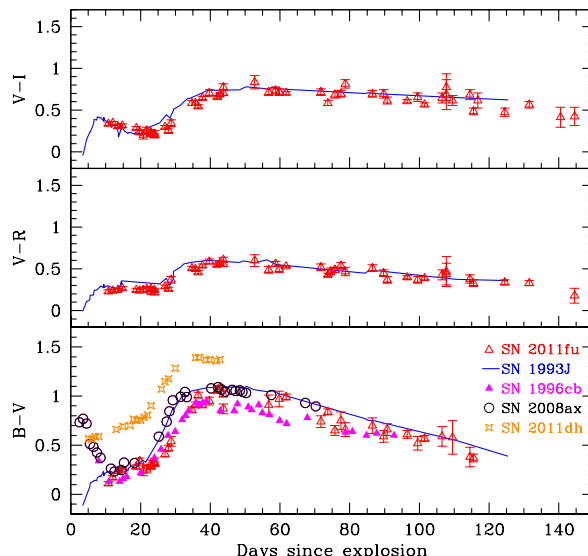
SN	Band	LC valley t_v (days)	Apparent magnitude at t_v	LC peak t_p (days)	Apparent magnitude at t_p
2011fu	U	15.51±4.34	17.67±0.42	22.93±3.64	17.43±3.34
	B	13.75±1.47	17.93±0.80	23.29±2.89	17.51±0.83
	V	12.87±1.69	17.45±1.32	24.96±2.01	16.95±0.42
	R	12.95±1.81	17.01±1.20	26.40±2.90	16.50±0.11
	I	13.50±1.89	16.86±0.67	26.64±2.80	16.41±0.32
1993J	U	10.33±1.52	11.94±0.76	–	–
	B	8.82 ±3.36	12.27±1.74	19.92±0.70	11.40±0.17
	V	8.96 ±1.41	11.89±1.14	21.67±0.66	10.87±0.12
	R	8.81 ±1.06	11.47±0.61	22.53±3.24	10.52±0.37
	I	9.17 ±1.58	11.25±0.93	23.06±1.91	10.39±0.21

(2010) reported similar observations for SN 2008ax). In the followings, we refer the first minimum of the LC (when the initial decline stops and the rise to the secondary maximum starts) as the “valley”.

To determine the epochs of the valleys (t_v , in days), the subsequent peaks (t_p , in days) and their corresponding brightness values, we fitted a third-order polynomial using a χ^2 minimization technique to the LCs of both SN 2011fu and SN 1993J. The errors in the fitting procedure were estimated by the error propagation method. We have taken 1993 March 27.5 as explosion date for SN 1993J (Wheeler et al., 1993). The derived values of t_v , t_p and corresponding brightness values for both SNe are listed in Table 4.

The values of t_v and t_p for both the SNe are similar within the errors in all the bands. However, for both SNe, the light curves peak earlier in blue bands than in the red bands (see Table 4) which is a common feature seen in CCSNe. By applying linear regression method, the decline and rising rates (in mag day⁻¹) were also estimated for three phases, i.e. the pre-valley (α_1), valley-to-peak (α_2) and after-peak phases (α_3). The results of the fitting are shown in Table 5. These values suggest that for SN 2011fu the pre-valley decay rates (α_1) are steeper (i.e. the decay is faster) at shorter wavelengths. This is also true for SN 1993J, where the decay rates (α_1) were even steeper. Thus, the initial LC decay of SN 1993J was steeper than that of SN 2011fu during this early phase (see also Barbon et al., 1995). Between valley to peak phase (α_2), the LC of SN 2011fu evolved with a similar rate in all the bands, but slower than that seen in case of SN 1993J. During the post-peak phase, the LCs gradually became flatter at longer wavelengths (see α_3 values in Table 5). This trend has also been observed for SN 1993J and other Type IIb SNe. The B -band LC of SN 2011fu between 50 and 100 days after explosion might even show a plateau, similar to SNe 1993J (see Fig. 3 of Lewis et al., 1994) and 1996cb (see Fig. 2 and the discussions of Qiu et al., 1999). The plateau-like behaviour of the U -band LC of SN 2011fu event is more prominent than the U -band LC of SN 1993J.

We also determined the Δm_{15} parameter for the V -band LCs of both SNe, Δm_{15} is defined as the decline in magnitude after 15 days post-maximum. We got $\Delta m_{15}(V) = 0.75$ mag for SN 2011fu which is slightly lower than that for SN 1993J ($\Delta m_{15}(V) = 0.9$ mag). Both of these values

**Figure 3.** Colour curves of SN 2011fu and other Type IIb SNe. Bottom panel: $B - V$ colour evolution for SNe 2011fu, 2011dh, 2008ax, 1996cb (symbols) and 1993J (blue line). Middle panel: $V - R$ colour for SN 2011fu and SN 1993J. Top panel: the same as below but for the $V - I$ colour.

are consistent with the mean $\Delta m_{15}(V) \sim 0.8 \pm 0.1$ mag for Type Ib/c SNe (Drout et al., 2011).

3.3 Colour evolution and reddening towards SN 2011fu

In Fig. 3, we compare the evolution of the optical colour indices of SN 2011fu with those of other Type IIb SNe. While constructing the colour curves, we interpolated the measured data points (listed in Table 2) wherever necessary. Before plotting the colours, reddening corrections were applied to all the bands. $E(B - V) = 0.068$ mag was adopted as the reddening due to Milky Way interstellar matter (ISM) in the direction of SN 2011fu (Schlegel et al., 1998). The empirical correlation given by Munari & Zwitter (1997) was used to estimate the SN host galaxy extinction based on the

Table 5. Magnitude decay rate (in mag day⁻¹) before valley (α_1), rising rate between valley to peak (α_2) and decay rate after the peak (α_3) in SN 2011fu and SN 1993J.

SN	Band	Decay rate before valley (α_1)	Rising rate between valley to peak (α_2)	Decay rate after peak (α_3)
2011fu	U	0.24 ± 0.05	-0.04 ± 0.01	0.13 ± 0.01
	B	0.15 ± 0.02	-0.05 ± 0.01	0.10 ± 0.01
	V	0.11 ± 0.03	-0.06 ± 0.01	0.05 ± 0.01
	R	0.09 ± 0.02	-0.05 ± 0.01	0.04 ± 0.01
	I	0.09 ± 0.02	-0.03 ± 0.01	0.02 ± 0.01
1993J	U	0.38 ± 0.03	–	–
	B	0.24 ± 0.02	-0.08 ± 0.01	0.11 ± 0.01
	V	0.24 ± 0.01	-0.10 ± 0.01	0.06 ± 0.01
	R	0.20 ± 0.01	–	–
	I	0.16 ± 0.01	-0.09 ± 0.01	0.05 ± 0.01

measured Na I D lines. For this purpose we calculated the weighted equivalent width (EW) of the un-resolved Na I D absorption feature in the three spectra (taken on 2011 Oct 01, 14 and 31, see the log in Table 3), resulted in EW (Na I D) $\sim 0.35 \pm 0.29$ Å. This corresponds to $E(B-V) \sim 0.15 \pm 0.11$ mag according to the relation given by Munari & Zwitter (1997). Finally, we adopted the sum of the two components, total $E(B-V) = 0.22 \pm 0.11$ mag as the reddening in the direction of SN 2011fu.

The bottom panel of Fig. 3 shows the $B-V$ colour evolution of SN 2011fu along with that of SNe 1993J (Lewis et al., 1994), 1996cb (Qiu et al., 1999), 2008ax (Pastorello et al., 2008) and 2011dh (Vinkó et al., 2012). It is seen in Fig. 3 that the colour curves of SN 2011fu are similar to those of the majority of well-observed Type IIb SNe, except SN 2011dh which looks being redder than the others.

Similar to SN 1993J, the initial $B-V$ colour of SN 2011fu increased (reddened) during the first 10 days (note that during the same phase SNe 2008ax and 1996cb showed the opposite trend). Between days +10 and +40, the $B-V$ colour continued to redden, then after day +40 it started to decrease and became bluer until the end of the our observations. This kind of colour evolution seems to be a common trend for Type Ib/c and IIb SNe. It may suggest that the SN ejecta became optically thin after 40 days. The $V-R$ (middle panel) and $V-I$ (upper panel) colour indices evolve with a similar trend as the $B-V$ colour.

3.4 Comparison of absolute magnitudes

The distribution of absolute magnitudes of CCSNe provides us information about their progenitors and explosion mechanisms. Richardson et al. (2002) made a comparative study of the distribution of peak absolute magnitudes in the B -band (M_B) for various SNe. They found that for normal and bright SNe Ib/c, the mean peak M_B values are -17.61 ± 0.74 and -20.26 ± 0.33 mag, respectively. The M_B values were found to be -17.56 ± 0.38 mag and -19.27 ± 0.51 mag for normal and bright Type II-L SNe, while for Type II-P and II-n SNe the M_B values were found to be -17.0 ± 1.12 mag and -19.15 ± 0.92 mag, respectively.

In a recent study by Li et al. (2011), absolute magni-

tudes of SNe Ib/c (Type Ib, Ic and Ib/c) and II were derived using LOSS samples and the average absolute magnitudes (close to R -band as claimed by authors, see discussions of Li et al. (2011)) were found to be -16.09 ± 0.23 mag and -16.05 ± 0.15 mag for SNe Ib/c and II respectively. In a similar study, Drout et al. (2011) also reported that R -band absolute magnitudes of SNe Ib and Ic peak around -17.9 ± 0.9 mag and -18.3 ± 0.6 mag respectively.

Fig. 4, shows the comparison of V -band absolute LC of SN 2011fu along with seven other well-observed Type IIb SNe i.e. 1993J (Lewis et al., 1994), 1996cb (Qiu et al., 1999), 2003bg (Hamuy et al., 2009), 2008ax (Pastorello et al., 2008), 2009mg (Oates et al., 2012), 2011dh (Vinkó et al., 2012) and 2011ei (Milisavljevic et al., 2012). For SN 2011fu, the distance $D = 77.9 \pm 5.5$ Mpc has been taken from the NED⁷ along with total $E(B-V) = 0.22 \pm 0.11$ mag as discussed in previous subsection. However, all other LCs presented in the figure have been corrected for interstellar extinctions and distance values collected from literature. Fig. 4, illustrates that the peak M_V for various Type IIb SNe has a range between ~ -16 mag and ~ -18.5 mag. In this distribution, SN 2011fu is the brightest from early to late epochs with a peak absolute magnitude of $M_V \sim -18.5 \pm 0.24$ mag.

4 BOLOMETRIC LIGHT CURVE

4.1 Construction of the bolometric light curve

The quasi-bolometric lightcurve ($UBVRI$) was computed by integrating the extinction-corrected flux⁸ in all 5-bands. The data were interpolated wherever it was necessary and total $UBVRI$ flux was integrated using a simple trapezoidal rule.

In Fig. 5, we compare the quasi-bolometric LC of SN 2011fu along with other three Type IIb events i.e. SNe

⁷ <http://ned.ipac.caltech.edu/>

⁸ Fluxes were corrected for interstellar reddening using the IDL program *ccm_unred.pro* available at ASTROLIB (<http://idlastro.gsfc.nasa.gov/ftp/>) by adopting $E(B-V) = 0.22$ mag for the total (Milky Way plus in-host) reddening and by assuming reddening law for the diffused interstellar medium ($R_v = 3.1$).

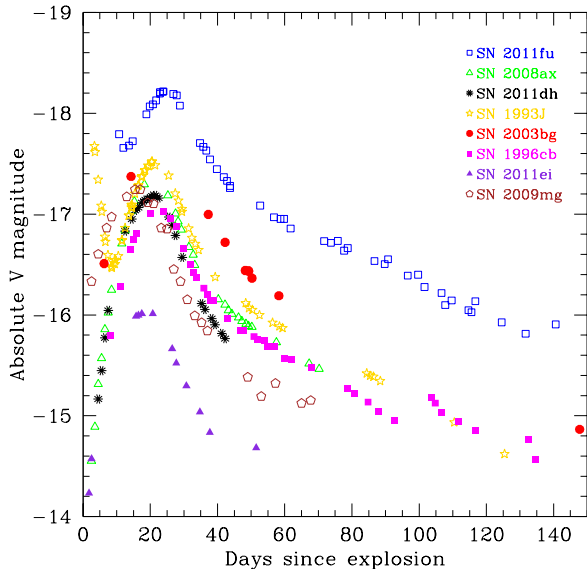


Figure 4. The M_V light curve of SN 2011fu is compared with those of other similar IIb events: SN 2011ei, 2011dh, 2009mg, 2008ax, 2003bg, 1996cb and 1993J.

1993J (Lewis et al., 1994), 2008ax (Pastorello et al., 2008) and SN 2011dh (Ergon, 2012). It is obvious that the shape of the quasi-bolometric LC of SN 2011fu is similar to that of SN 1993J. However, SN 2011fu is more luminous in comparison with the other SNe during the observed phases.

The un-observed part of the bolometric LC in the Infrared was approximated by assuming blackbody flux distributions fitted to the observed R - and I -band fluxes for each epoch. At first, we used the Rayleigh-Jeans approximation for the fluxes redward of the I -band, and integrated the flux distribution between the I -band central wavelength and infinity. This resulted in an analytic estimate for the IR (infrared) contribution as $L_{IR} \approx \lambda_I \cdot F_I / 3$, where λ_I and F_I are the I -band central wavelength and monochromatic flux, respectively. Second, we fitted a blackbody to the R - and I -band fluxes at each epoch, and numerically integrated the fitted blackbody flux distributions from the I -band to radio wavelengths (~ 1 mm). These two estimates gave consistent results within a few percent, which convinced us that they are more-or-less realistic estimates of the IR-contribution. Because the R -band fluxes may also be affected by the presence of $H\alpha$, we adopted the result of the first, analytic estimate as the final result. The comparison of the integrated $UBVRI$ - and IR-fluxes showed that the IR-contribution was ~ 20 percent at the earliest observed phases, but it increased up to ~ 50 percent by day +40 and stayed roughly constant after that.

4.2 Bolometric light curve modelling

The bolometric light curve (see subsection 4.1) was fitted by the semi-analytic light curve model of Arnett & Fu (1989) (see also Chatzopoulos et al., 2009). This model assumes homologously expanding spherical ejecta having constant opacity, and solves the photon diffusion equation taking into account the laws of thermodynamics. This approach was

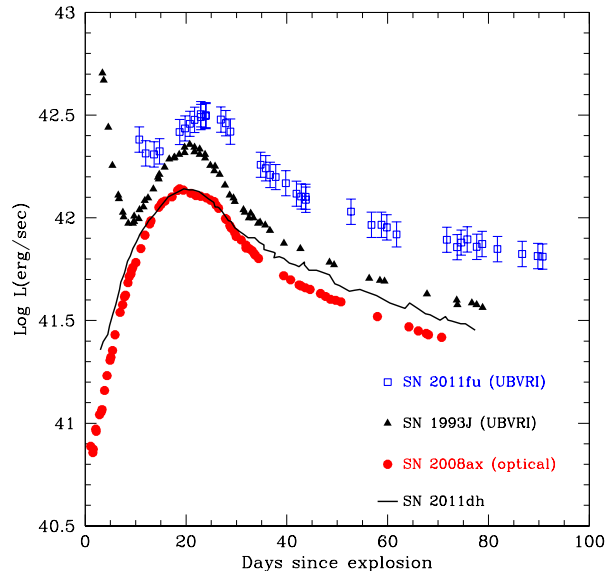


Figure 5. The bolometric light curve of SN 2011fu compared with similar Type IIb events SN 1993J (Lewis et al., 1994), SN 2008ax (Pastorello et al., 2008) and SN 2011dh (Ergon et al. 2012)

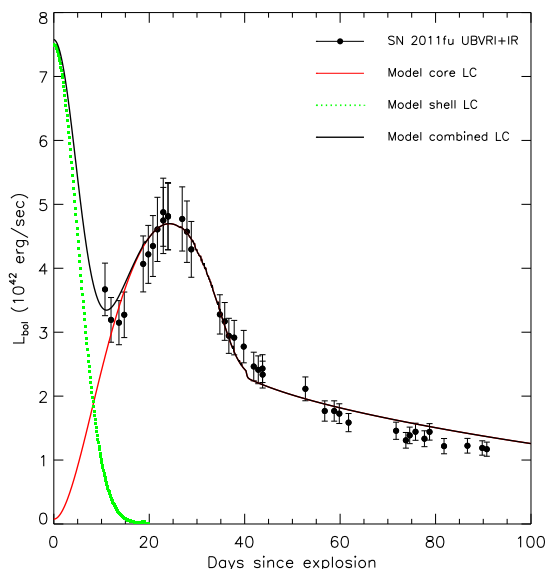
first introduced by Arnett (1980) and Arnett (1982), and further extended by Arnett & Fu (1989) by taking into account the rapid change of the opacity due to recombination. The extended diffusion-recombination model was successfully applied to describe the observed light curve of SN 1987A assuming realistic physical parameters (Arnett & Fu, 1989).

The bolometric LC of SN 2011fu is qualitatively similar to that of SN 1987A, because of the presence of the rapid initial decline and the secondary bump, after which the LC settles down onto the radioactive tail due to the ^{56}Co -decay. This early LC decline is not unusual in Type IIb SNe (however, see Fig. 2 at early epoch where we compare the LCs of SN 2011fu with SN 1993J), and it is usually modelled by a two-component ejecta configuration: a dense compact core and a more extended, lower density envelope on top of the core (Bersten et al., 2012). The fast, initial decline is thought to be due to the radiation of the cooling outer envelope (which was initially heated by the shock wave passing through it after the explosion), while the secondary bump is caused by the photons diffusing slowly out from the inner, denser ejecta which is mainly heated from inside by the radioactive decay of $^{56}\text{Ni} \rightarrow ^{56}\text{Co} \rightarrow ^{56}\text{Fe}$. After the secondary maximum, the decline of the LC is faster than the rate of the radioactive decay, which may be due to a recombination front moving inward into the ejecta, similar to the condition at the end of the plateau phase in Type II-P SNe.

In order to simulate this kind of LC behavior, we slightly modified the original diffusion-recombination model of Arnett & Fu (1989). Instead of having a H-rich, one-component ejecta, we added an extended, low-density, pure H envelope on top of a denser, He-rich core. Following Arnett & Fu (1989), we also assumed that the opacity is due to only Thompson-scattering, and it is constant in both the envelope and the core. Because the envelope was thought to contain only H, $\kappa = 0.4 \text{ cm}^2 \text{ g}^{-1}$ was selected as the Thompson-scattering opacity for this layer, while $\kappa = 0.24$

Table 6. Log of parameters derived from bolometric light curve modelling, discussed in section 4.2.

Parameters	He-core	H-envelope	remarks
R_{prog} (cm)	2×10^{11}	1×10^{13}	progenitor radius
M_{ej} (M_{\odot})	1.1	0.1	ejecta mass
κ_T (cm^2g^{-1})	0.24	0.4	Thompson scattering opacity
M_{Ni} (M_{\odot})	0.21	–	initial nickel mass
E_{kin} (10^{51} erg)	2.4	0.25	ejecta kinetic energy
$E_{th}(0)$ (10^{51} erg)	1.0	0.3	ejecta initial thermal energy

**Figure 6.** Comparison of the observed bolometric LC (dots) with the best-fit two-component diffusion-recombination model. The red and green curves show the contribution from the He-rich core and the low-mass H-envelope, respectively, while the black line gives the combined LC.

cm^2g^{-1} was applied for the inner region to reflect its higher He/H ratio.

The system of differential equations given by Arnett & Fu (1989) were then solved by simple numerical integration (assuming a short, $\Delta t = 1$ s timestep which was found small enough to get a reasonable and stable solution). Because the photon diffusion timescale is much lower in the envelope than in the core, the contribution of the two regions to the overall LC is well separated: during the first few days the radiation from the outer, adiabatically cooling envelope dominates the LC, while after that only the photons diffusing out from the centrally heated inner core contribute. Thus, the sum of these two processes determines the final shape of the LC.

Because of the relatively large number of free parameters, we have not attempted a formal χ^2 minimization while fitting the model to the observations. Instead, we searched for a qualitative agreement between the computed and observed bolometric LCs. The parameters of our final, best-fit-by-eye model are collected in Table 6, while the LCs are plotted in Fig. 6.

It is seen that the best-fit model consists of a dense, $1 M_{\odot}$ He-rich core and a more extended, low-mass ($0.1 M_{\odot}$)

H-envelope. This is very similar to the progenitor configuration found by Bersten et al. (2012) when modelling the LC of another Type IIb event, SN 2011dh, although they assumed a more massive ($\sim 3 M_{\odot}$) He-core. Nevertheless, it was concluded by Bersten et al. (2012) and confirmed by the present study that the secondary bump is entirely due to radiation coming from the dense inner core of the ejecta, and the outer extended envelope is only responsible for the initial fast decline of the LC. The estimated ejecta mass for SN 2011fu, $\sim 1.1 M_{\odot}$ is consistent with the observed rise time (~ 24 days) to the secondary maximum of the LC (see Eq.10 of Chatzopoulos et al., 2012). The parameters in Table 6 are also qualitatively similar to the ones derived by Young et al. (1995) for modelling the LC of SN 1993J.

There are a number of caveats in the simple diffusion-recombination model used above, which naturally limit the accuracy of the derived physical parameters. The most obvious limitation is the assumption of constant opacity in the ejecta. The pre-selected density and temperature profiles in the ejecta (assumed as exponential functions) are also strong simplifications, but they enable the approximate, semi-analytic treatment of the complex problem of radiative diffusion, as shown by Arnett & Fu (1989). Thus, the parameters in Table 6 can be considered only as order-of-magnitude estimates, which could be significantly improved by more sophisticated modelling codes (e.g. Bersten et al., 2012).

5 SPECTRAL ANALYSIS

Properties of the SN 2011fu ejecta were investigated with the multi-parametric resonance scattering code SYNOW (Fisher et al., 1997) (see also Branch et al., 2002; Baron et al., 2005; Elmhamdi et al., 2006). The evolution of temperature and velocities of layers were traced through several months of spectral observations. The SYNOW code is based on several assumptions: spherical symmetry; homologous expansion of layers ($v \sim r$); sharp photosphere producing a blackbody spectrum and associated with a shock wave at early stages.

5.1 Comparison between observed and synthetic spectra

In the photospheric phase the spectral lines with P Cygni profiles are formed by resonance scattering in a shell above the optically thick photosphere which produces the continuum (see Branch et al., 2001). On the other hand, during the nebular phase the ejecta is transparent (optically thin)

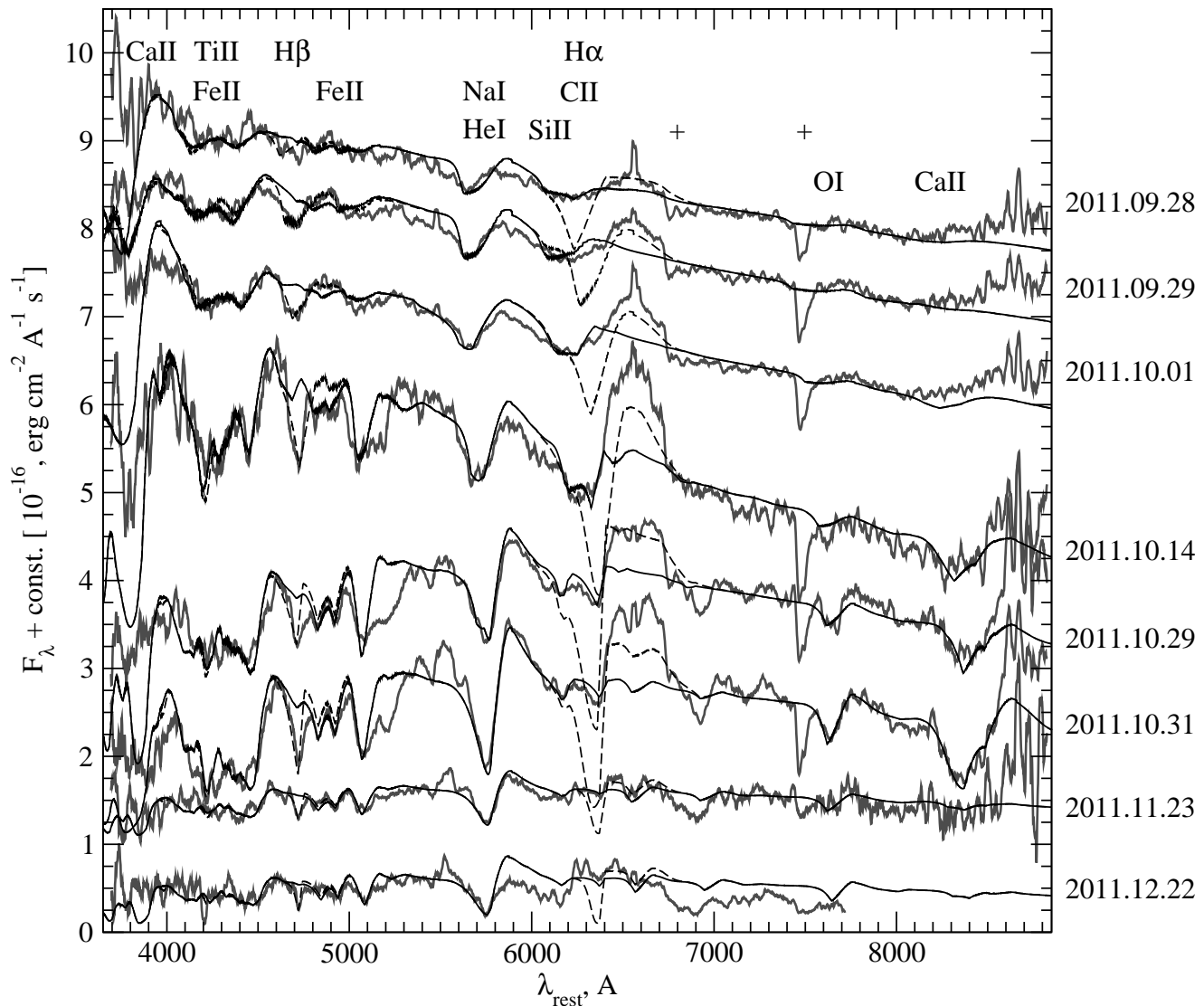


Figure 7. The evolution of the SN 2011fu spectra (grey thick curves, smoothed by a 20Å-wide window function) overplotted with SYNOW models. The main models are shown by the solid black line. The models with $H\beta$ fitting are shown as dashed black line. The most conspicuous ions are marked. Atmospheric lines are marked with “+”.

in the optical wavelength range. In this case the spectrum is dominated by strong emission features including forbidden lines. Each of these two phases of SN evolution can be explained with individual approximations and the modelling of the observed spectra should be made with different synthetic codes. There is no sharp boundary between these two phases. No strong transition to the nebular phase with conspicuous emission features can be seen in the observed spectra of SN 2011fu (Fig. 7). The shape of lines remains the P Cyg profile, which suggests that they are formed by resonance scattering, as assumed in SYNOW. Thus, we modelled all spectra of SN 2011fu with this code. Before modelling, all spectra have been corrected for redshift (see Sect. 2).

The strong emission component of the $H\alpha$ line (probably with the CII and SiII contamination) can not be fully fitted in the terms of the SYNOW code. We focused primarily on the absorption parts of P Cyg line profiles which provide information about the expansion velocities of different line-

forming layers. The SYNOW code allows the usage of different optical depth (i.e. density) profiles. Two of them are the exponential profile with the parameter of e-folding velocity “ v_e ” ($\tau \propto \exp(-v/v_e)$) which can be adjusted for each ion, and the power-law profile with the index “ n ” ($\tau \propto v^{-n}$) which is applied to all ions in the model. We checked both cases and found that the exponential law is more suitable for our spectra. The original paper of the SYNOW developers and further studies showed a possibility of spectral features which can be detached or undetached from the photosphere. These two configurations produce different shapes for the line profiles, which was described in the paper by Sonbas et al. (2008).

The first three observed spectra are separated by only one and two days. That is why they can be modelled by similar sets of parameters (see Table 7). Even the spectrum obtained on Oct 14 has a similar continuum slope ($T_{bb} \approx 6500 - 6700K$). To verify the pseudo-photospheric

temperature derived by `SYNOW` modelling, we also evaluated the colour temperature (T_{col}) of the SN using the models of Dessart & Hillier (2005) and Bersten & Hamuy (2009). We used the $B - V$ colours for those epochs where spectra were available, and then estimated the temperature from the corresponding $B - V$ colour. Both of these temperature estimates seem to be consistent except for the spectra taken on Oct 14 and Dec 22, 2011.

5.2 Velocity of the pseudo-photosphere

The velocity of the pseudo-photosphere (an optically thick layer, the surface of last scattering for continuum photons) can be located by velocities of heavy elements such as Fe II and Ti II, which may produce optically thin spectral features. However, during the very early phases these features are very weak and blended. Therefore, fitting the first three spectra by these ions gives a wide range of possible photospheric velocities, extending from 13 000 to 19 000 km s⁻¹. The most prominent, narrow absorption feature in these spectra is the feature near 5650Å produced by He I (which may be blended with Na I D). This feature is useful to better constrain the velocity at the pseudo-photosphere, and decrease the uncertainty of this parameter at the earliest phases. All velocities derived this way are shown in the V_{phot} column of Table 7.

5.3 Hydrogen and the 6200Å absorption feature

The wide absorption feature near 6200Å can be fitted with the help of a high-velocity H-layer (up to $V \sim 20\,000$ km s⁻¹) which may be detached from the pseudo-photosphere. On the other hand, fitting the emission peak of $H\alpha$ with `SYNOW` needs lower velocities, but those models cannot reproduce the absorption profile (see Fig. 7). In the $V(H\alpha)$ column of Table 7 we list the results from the latter, more conservative solution.

The broad absorption at 6200Å can be also explained with the presence of the C II ion having a high-velocity almost identical to that of $H\alpha$. Moreover, C II also produces a small feature near 4400Å. This feature can constrain the reference optical depth (τ) for ionized carbon. But the contamination from heavy elements in the blue region makes the fitting of the C II 4400Å feature uncertain. Thus, the presence of carbon cannot be confirmed from these spectra.

It is also possible to explain the 6200Å feature by singly ionized silicon. In this case the velocity of Si II must be very low. On the other hand, it is expected that the velocity of Si II should be equal or only slightly higher than the photospheric velocity. It turned out that only the blue wing of this wide feature can be fitted by Si II. Although the small absorption near 5880 Å might be explained by the presence of Si II, the observed shape of the 6200Å feature does not confirm this hypothesis.

In order to look for other possibilities, we also checked different blends of H, Si II, C II and some other ions with different velocities (assuming undetached as well as detached line formation) in our models. At the early phases the range of derived velocities turned out to be wide due to the lack of observable spectral features formed close to the photosphere, as discussed above. At the late phases, the wide absorption near 6200Å splitted into at least three separate

Table 7. Velocities of the pseudo-photosphere, $H\alpha$ and $H\beta$ for different epochs of SN 2011fu evolution, derived with `SYNOW`. We assumed that the photospheric velocity (V_{phot}) is equal to the velocity of Fe II. All velocities are given in km s⁻¹. T_{bb} is the blackbody temperature of the pseudo-photosphere in Kelvin degrees. The colour temperature (T_{col}) derived from effective temperature – colour relations (see Dessart & Hillier, 2005; Bersten & Hamuy, 2009) is given in last column.

UT Date (yyyy/mm/dd)	V_{phot} (Fe II)	$V(H\alpha)$	$V(H\beta)$	T_{bb}	T_{col}
2011/09/28	14000	16000	16000	6700	6952
2011/09/29	14000	16000	14000	6500	6476
2011/10/01	11000	15000	11000	6500	6052
2011/10/14	8000	11000	8500	6700	5791
2011/10/29	6200	9500	9500	5000	4698
2011/10/31	6000	9000	9000	5000	4795
2011/11/23	6000	9000	9000	5000	5094
2011/12/22	5000	9000	9000	5000	5718

features (6100Å, 6200Å, 6350Å). These features might be explained as a line formation effect for $H\alpha$ in layers with different velocities or the appearance of blending due to ions mentioned above. Unfortunately, no firm conclusion can be drawn based on the simple parametric models that `SYNOW` can produce.

The deep absorption near 4700Å can be naturally explained identifying it as the $H\beta$ line. We fitted this line and the $H\alpha$ line independently because they cannot be modeled by the same set of parameters: τ , v_{phot} and v_e (see also Quimby et al., 2007). From Table 7 it is visible that for the spectra obtained before Oct 29 the fitting of $H\alpha$ needs higher velocities than the fitting of $H\beta$. Although both the $H\alpha$ and $H\beta$ velocities declined in time, the formation of the absorption component of $H\alpha$ stayed at higher velocities than for $H\beta$. This may suggest that $H\alpha$ remained optically thick for a longer time than $H\beta$ in the expanding, diluting H-rich envelope.

5.4 Other ions

To fit the main features in the spectra, we included the following elements and ions in `SYNOW`: H, Fe II, Ti II, Na I, Si II, O I and Ca II. Some models were also computed containing the following elements and ions as alternatives: C II, He I, Fe I, Ti I, Sc II, Mg I and the consistency of these ions were cross-examined with Hatano et al. (1999). The heavier atoms/ions should have velocities close to v_{phot} but the lighter ones may be detached due to e.g. stratification of elements in the ejecta.

In the followings, we show some possibilities to explain these features in the observed spectra. Weak features near 4810Å and 6370Å can be explained by the presence of low-velocity He I. He can also be found as a blend with Na I in the deep absorption near 5650Å mentioned above, and as a blend with Ti II and Fe II near 4300Å. However, the velocity of He I may be higher than the photospheric velocity. Even in this case, the presence of He can explain all these features.

A small absorption in the blue wing of $H\alpha$ at 6630Å could be modeled by He I or low-velocity C II. The feature near 5050Å could be fitted with Mg I as well. The Ca II H+K

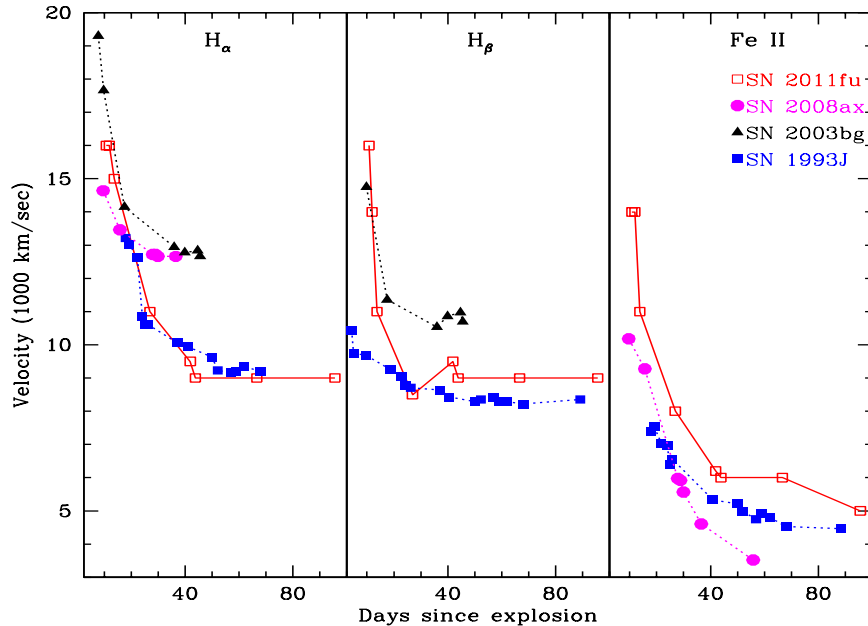


Figure 8. The evolution $H\alpha$, $H\beta$ and Fe II line velocities by fitting SYNOW model (see Table 7). Photospheric velocities for SN 2011fu, 2003bg (Hamuy et al., 2009), 1993J (Lewis et al., 1994; Barbon et al., 1995) and 2008ax (Pastorello et al., 2008) are shown. The symbols of SN 2011fu are connected with lines, those of other SNe with dotted lines.

feature cannot be fitted well around 3730\AA , because this regime is at the blue end of our observed spectra and all of them are very noisy at these wavelengths. But the absorption feature near 8400\AA is compatible with the Ca II IR-triplet.

5.5 Results of spectral modelling

Almost all spectral features are described well with elements and ions which are usually applied in the case of Type IIb SNe. However, the strong emission of $H\alpha$ dominating during intermediate epochs can not be fully fitted with the models applied.

The fitting of redder and especially bluer parts has some uncertainties due to strong blending of metal lines such as Ca II, Ti II, Fe II and others. Even without precise modelling, all spectral sequences can be divided into two groups: the first four spectra (up to Oct 14) which are fitted with models with the blackbody temperature $T_{bb} \approx 6500 - 6700$ K and the following four spectra with $T_{bb} \approx 5000$ K.

Generally, the modelling of the SN 2011fu spectra shows the decline of the photospheric velocities up to ~ 40 days after the explosion (see Fig. 8). Then, all velocities remain approximately at the same, stable level. This behaviour was also described in previous works on CCSNe (Branch et al., 2002; Quimby et al., 2007; Moskvitin et al., 2010). In Fig. 8 we plot the velocities of $H\alpha$, $H\beta$ and Fe II for SN 2011fu, SN 2008ax, SN 2003bg and SN 1993J, illustrating this effect.

6 METALLICITY-BRIGHTNESS COMPARISON OF HOST GALAXIES

In several earlier studies of CCSNe hosts, it has been already mentioned that various SNe subtypes occur in different environments (see Prieto et al., 2008; Anderson et al., 2010; Arcavi et al., 2010; Modjaz et al., 2011; Kelly & Kirshner, 2012; Sanders et al., 2012). Metallicity is a key factor in all these studies. Recent studies by Arcavi et al. (2010) and Prieto et al. (2008) found that SN Ib/c host galaxies are metal-rich as compared to SN II hosts. Modjaz et al. (2011) found that SNe Ic are more metal-rich (up to 0.20 dex) than SNe Ib. In a similar study on SNe Ib/c locations Leloudas et al. (2011) found a smaller gap between the two metallicities (the environment of SNe Ic is richer by ~ 0.08 dex than Ib). In a recent study with a different approach (using local emission-line for metallicity estimates), where 74 H II regions in CCSNe hosts were analyzed, Anderson et al. (2010) did not find difference between the metallicities of these two environments.

Type IIb host galaxies have been claimed to be more metal-poor than those of SNe Ib or Ic (see Arcavi et al., 2010; Kelly & Kirshner, 2012), although in another recent study which is based on the SN sample from untargeted searches (although with a rather small sample of 8 SNe IIb) Sanders et al. (2012) found that the median metallicity of both SNe Ib and IIb host galaxies is very similar.

In an attempt to understand the metallicity scenario for the SN 2011fu host galaxy, we collected the latest sample of metallicity data for hosts of CCSNe, and their absolute magnitudes in the B -band from litera-

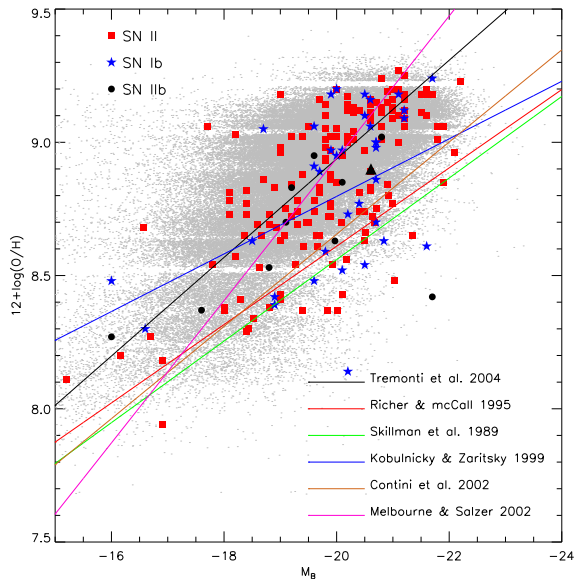


Figure 9. Metallicity-luminosity relation for various types of SNe host galaxies. The tiny dots belong to all galaxies used by Prieto et al. (2008) (This catalog is based on SDSS DR4 Adelman-McCarthy et al., 2006, database). Red squares are Type II, stars are Type Ib/c and black dots are Type Iib SNe, respectively. The analytic relations collected from several papers (see text) are also over-plotted. SN 2011fu host metallicity is denoted by a black triangle.

tures (Leloudas et al., 2011; Modjaz et al., 2011; Stoll et al., 2012) and available online⁹. In Fig. 9, the data for these host galaxies (36 for Ib, 15 for Iib and 167 for remaining II SNe) were then overplotted to the sample containing all star forming galaxies from SDSS DR4 (This sample was taken from Prieto et al., 2008). The relations between metallicity and M_B for galaxies from several papers are also over-plotted (Skillman et al., 1989; Richer & McCall, 1995; Kobulnicky & Zaritsky, 1999; Contini et al., 2002; Melbourne & Salzer, 2002; Tremonti et al., 2004).

We estimated the metallicity of the host of SN 2011fu using the relation given by Garnett (2002) (see their equation 6). We considered $M_B = -20.62$ mag for UGC 01626 from HyperLeda. The calculated $\log(O/H) + 12$ for UGC 01626 is $8.90^{+0.10}_{-0.06}$. This value is slightly higher than $\log(O/H) + 12 = 8.55$ (Arcavi et al., 2010) and $\log(O/H) + 12 = 8.44$ (Sanders et al., 2012) for SN type II sample. Our analysis using most updated sample of absolute magnitudes and metallicities of CCSNe host galaxies also supports the results described in Sanders et al. (2012). However, it is noticeable that methods used to determine metallicities are based on statistical samples, affected by incompleteness of the sample and should be used with caution.

7 CONCLUSIONS

We present a comprehensive *UBVRI* photometric and low-resolution spectroscopic monitoring of the Type Iib SN

2011fu. To date, only a handful of SNe belonging to this class have been observed and studied in detail.

To the best of our knowledge, our photometric and spectroscopic observations described here are the earliest ones reported for this event. The early photometric observations strongly suggest the presence of the early-time decline of the light curve (which is thought to be related to the shock break-out phase) as seen in case of SN 1993J. The early-time LC decay rate (α_1) of this SN is slower than that derived for SN 1993J in all the bands. The rising rates between the LC valley to peak (α_2) observed in SN 2011fu is also somewhat slower than in SN 1993J. However, the post peak LC decay rate (α_3) are similar in the two events.

The colour evolutions of SN 2011fu were studied using our *UBVRI* band observations. Our data showed that during the very early phases the $B - V$ colour was very similar to that in SN 1993J. A similar trend has been found in the $V - R$ and $V - I$ colours as well. The evolution of these three colours after +40 days were also similar to those seen in other CCSNe. The V -band absolute magnitudes of a sample of 8 Type Iib SNe were compared after applying proper extinction corrections and taking into account distances collected from the literature. In this sample, SN 2011fu seems to be the most luminous event. However, the peak V -band absolute magnitude of SN 2011fu is not an outlier when is compared to the peak brightness of CCSNe of other types.

The quasi-bolometric LC of SN 2011fu was assembled using our *UBVRI* data and accounting for the IR contribution as specified in Section 4. The comparison of these data with other known Type Iib SNe also shows that SN 2011fu is the brightest Type Iib SN in the sample. The bolometric LC was modeled by applying a semi-analytical model of Arnett & Fu (1989). This model suggests a $1.1 M_\odot$ He-rich core and an extended, low-mass ($\sim 0.1 M_\odot$) H-envelope as the progenitor of SN 2011fu, similar to that of SN 2011dh. However, the progenitor radius of SN 2011fu ($\sim 1 \times 10^{13}$ cm) turned out to be smaller than that of SN 1993J ($\sim 4 \times 10^{13}$ cm) (Woosley et al., 1994). The ejected nickel mass for SN 2011fu was $\sim 0.21 M_\odot$, higher than that of SN 1993J ($0.07 - 0.11 M_\odot$).

The spectra of SN 2011fu taken at eight epochs were analyzed using the multi-parameter resonance scattering code *SYNOW*. The derived parameters describe the evolution of the velocities related to various atoms/ions and the variation of the blackbody temperature of the pseudo-photosphere. The photospheric velocities at the early epochs were higher than that of other Type Iib SNe. The pseudo photospheric temperatures were found to be between 6700 K and 5000 K, decreasing from initial to later phases. The temperatures from *SYNOW* were also checked by comparing them with colour temperatures calculated from $B - V$ vs T_{eff} relations (Bersten & Hamuy, 2009; Dessart & Hillier, 2005). These different temperature estimates were found being consistent. The appearance of the main observed spectral features were also successfully modeled with *SYNOW* by assuming H, He I and various metals (mostly Fe II, Ti II and Ca II), which are typical of CCSNe spectra. The estimated value of the metallicity of the host galaxy of SN 2011fu is $8.90^{+0.10}_{-0.06}$ similar to those for other Type Iib SNe.

⁹ www.astro.princeton.edu/~jprieto/snhosts/

ACKNOWLEDGEMENTS

We thank the referee, Andrea Pastorello for a critical reading of the paper and several useful comments and suggestions, which greatly improved the scientific content of the manuscript. We are also thankful to the observers at the Aryabhata Research Institute of observational sciences (ARIES) who provided their valuable time and support for the observations of this event. We are thankful to the staffs of 1.3m DFOT and HCT for their kind cooperation. SBP acknowledge the support of Indo-Russian (DST-RFBR) project No. INT/RFBR/P-100 for this work. This work was also supported by the following grants: The RFBR grant 11-02-12696-IND-a; the program no. 17 “Active processes in galactic and extragalactic objects” of the Department of Physical Sciences of the Russian Academy of Sciences and grants No. 14.B37.21.0251 and No. 14.A18.21.1179 from FTP of the RF Ministry of education and science. The work of JV and AO has been supported by Hungarian OTKA Grant K76816. BK is thankful to Eswarajah, C. for his help during writing of this article. BK also acknowledge the support of Actions de Recherche Concertées (ARC). This research has made use of the NASA/IPAC Extragalactic Database (NED) which is operated by the Jet Propulsion Laboratory, California Institute of Technology, under contract with the National Aeronautics and Space Administration. We acknowledge the usage of the HyperLeda database (<http://leda.univ-lyon1.fr>).

REFERENCES

- Adelman-McCarthy J. K., Agüeros M. A., Allam S. S., et al., 2006, *ApJS*, 162, 38
- Aldering G., Humphreys R. M., Richmond M., 1994, *AJ*, 107, 662
- Anderson J. P., Covarrubias R. A., James P. A., Hamuy M., Haberman S. M., 2010, *MNRAS*, 407, 2660
- Anderson J. P., James P. A., 2009, *MNRAS*, 399, 559
- Arcavi I., Gal-Yam A., Kasliwal e. a. M. M., et al., 2010, *ApJ*, 721, 777
- Arcavi I., Gal-Yam A., Yaron O., et al., 2011, *ApJ*, 742, L18
- Arnett W. D., 1980, *ApJ*, 237, 541
- Arnett W. D., 1982, *ApJ*, 253, 785
- Arnett W. D., Fu A., 1989, *ApJ*, 340, 396
- Barbon R., Benetti S., Cappellaro E., Patat F., Turatto M., Iijima T., 1995, *A&AS*, 110, 513
- Baron E., Nugent P. E., Branch D., Hauschildt P. H., 2005, in 1604-2004: Supernovae as Cosmological Lighthouses, edited by M. Turatto, S. Benetti, L. Zampieri, W. Shea, vol. 342 of *Astronomical Society of the Pacific Conference Series*, 351
- Benetti S., Cappellaro E., Turatto M., Pastorello A., 2000, *IAU Circ.*, 7375, 2
- Bersten M. C., Benvenuto O. G., Nomoto K., et al., 2012, *ApJ*, 757, 31
- Bersten M. C., Hamuy M., 2009, *ApJ*, 701, 200
- Bietenholz M. F., Brunthaler A., Soderberg A. M., et al., 2012, *ApJ*, 751, 125
- Blinnikov S. I., Eastman R., Bartunov O. S., Popolitov V. A., Woosley S. E., 1998, *ApJ*, 496, 454
- Blondin S., Tonry J. L., 2007, *ApJ*, 666, 1024
- Branch D., Baron E., Jeffery D. J., 2001, *ArXiv Astrophysics e-prints*, arXiv:astro-ph/0111573
- Branch D., Benetti S., Kasen D., et al., 2002, *ApJ*, 566, 1005
- Chatzopoulos E., Wheeler J. C., Vinko J., 2009, *ApJ*, 704, 1251
- Chatzopoulos E., Wheeler J. C., Vinko J., 2012, *ApJ*, 746, 121
- Chevalier R. A., 1992, *ApJ*, 394, 599
- Chevalier R. A., Fransson C., 2008, *ApJ*, 683, L135
- Chevalier R. A., Soderberg A. M., 2010, *ApJ*, 711, L40
- Chornock R., Filippenko A. V., Li W., et al., 2011, *ApJ*, 739, 41
- Ciabattari F., Mazzoni E., Jin Z., et al., 2011, *Central Bureau Electronic Telegrams*, 2827, 1
- Clocchiatti A., Wheeler J. C., Phillips M. M., et al., 1997, *ApJ*, 483, 675
- Contini T., Treyer M. A., Sullivan M., Ellis R. S., 2002, *MNRAS*, 330, 75
- Crockett R. M., Eldridge J. J., Smartt S. J., et al., 2008, *MNRAS*, 391, L5
- Dessart L., Hillier D. J., 2005, *A&A*, 437, 667
- Drout M. R., Soderberg A. M., Gal-Yam A., et al., 2011, *ApJ*, 741, 97
- Elmhamdi A., Danziger I. J., Branch D., Leibundgut B., Baron E., Kirshner R. P., 2006, *A&A*, 450, 305
- Ergon M., 2012, in preparation
- Falk S. W., Arnett W. D., 1977, *ApJS*, 33, 515
- Filippenko A. V., 1988, *AJ*, 96, 1941
- Filippenko A. V., 1997, *ARA&A*, 35, 309
- Filippenko A. V., Chornock R., 2003, *IAU Circ.*, 8084, 4
- Fisher A., Branch D., Nugent P., Baron E., 1997, *ApJ*, 481, L89
- Fryer C. L., 1999, *ApJ*, 522, 413
- Gal-Yam A., Kasliwal M. M., Arcavi I., et al., 2011, *ApJ*, 736, 159
- Garnett D. R., 2002, *ApJ*, 581, 1019
- Hamuy M., Deng J., Mazzali P. A., et al., 2009, *ApJ*, 703, 1612
- Hatano K., Branch D., Fisher A., Millard J., Baron E., 1999, *ApJS*, 121, 233
- Heger A., Fryer C. L., Woosley S. E., Langer N., Hartmann D. H., 2003, *ApJ*, 591, 288
- Horesh A., Stockdale C., Fox D. B., et al., 2012, *ArXiv e-prints*, arXiv:1209.1102 [astro-ph.CO]
- Horne K., 1986, *PASP*, 98, 609
- Kelly P. L., Kirshner R. P., 2012, *ApJ*, 759, 107
- Kobulnicky H. A., Zaritsky D., 1999, *ApJ*, 511, 118
- Krauss M. I., Soderberg A. M., Chomiuk L., et al., 2012, *ApJ*, 750, L40
- Kumar B., Sagar R., Rautela B. S., Srivastava J. B., Srivastava R. K., 2000, *Bulletin of the Astronomical Society of India*, 28, 675
- Landolt A. U., 2009, *AJ*, 137, 4186
- Leloudas G., Gallazzi A., Sollerman J., et al., 2011, *A&A*, 530, A95
- Lewis J. R., Walton N. A., Meikle W. P. S., et al., 1994, *MNRAS*, 266, L27
- Li W., Leaman J., Chornock R., et al., 2011, *MNRAS*, 412, 1441

- Martí-Vidal I., Tudose V., Paragi Z., et al., 2011, *A&A*, 535, L10
- Maund J. R., Fraser M., Ergon M., et al., 2011, *ApJ*, 739, L37
- Maund J. R., Smartt S. J., Kudritzki R. P., Podsiadlowski P., Gilmore G. F., 2004, *Nature*, 427, 129
- Maurer I., Mazzali P. A., Taubenberger S., Hachinger S., 2010, *MNRAS*, 409, 1441
- Mazzali P. A., Deng J., Hamuy M., Nomoto K., 2009, *ApJ*, 703, 1624
- Melbourne J., Salzer J. J., 2002, *AJ*, 123, 2302
- Milisavljevic D., Margutti R., Soderberg A. M., et al., 2012, *ArXiv e-prints*, arXiv:1207.2152 [astro-ph.HE]
- Modjaz M., Kewley L., Bloom J. S., Filippenko A. V., Perley D., Silverman J. M., 2011, *ApJ*, 731, L4
- Monard L. A. G., 2007, *Central Bureau Electronic Telegrams*, 845, 1
- Moskvitin A. S., Sonbas E., Sokolov V. V., Fatkhullin T. A., Castro-Tirado A. J., 2010, *Astrophysical Bulletin*, 65, 132
- Munari U., Zwitter T., 1997, *A&A*, 318, 269
- Nakar E., Sari R., 2010, *ApJ*, 725, 904
- Oates S. R., Bayless A. J., Stritzinger M. D., et al., 2012, *MNRAS*, 424, 1297
- Pastorello A., Kasliwal M. M., Crockett R. M., et al., 2008, *MNRAS*, 389, 955
- Podsiadlowski P., Joss P. C., Hsu J. J. L., 1992, *ApJ*, 391, 246
- Prieto J., 2009, *Central Bureau Electronic Telegrams*, 2087, 1
- Prieto J. L., Stanek K. Z., Beacom J. F., 2008, *ApJ*, 673, 999
- Puls J., Vink J. S., Najarro F., 2008, *A&A Rev.*, 16, 209
- Qiu Y., Li W., Qiao Q., Hu J., 1999, *AJ*, 117, 736
- Quimby R. M., Wheeler J. C., Höflich P., Akerlof C. W., Brown P. J., Rykoff E. S., 2007, *ApJ*, 666, 1093
- Richardson D., Branch D., Baron E., 2006, *AJ*, 131, 2233
- Richardson D., Branch D., Casebeer D., Millard J., Thomas R. C., Baron E., 2002, *AJ*, 123, 745
- Richer M. G., McCall M. L., 1995, *ApJ*, 445, 642
- Richmond M. W., Treffers R. R., Filippenko A. V., et al., 1994, *AJ*, 107, 1022
- Roming P., Prieto J., Milne P. A., 2009a, *Central Bureau Electronic Telegrams*, 2093, 1
- Roming P., Pritchard T., Brown P., et al., 2010, in *American Astronomical Society Meeting Abstracts #215*, vol. 42 of *Bulletin of the American Astronomical Society*, 342.03
- Roming P. W. A., Pritchard T. A., Brown P. J., et al., 2009b, *ApJ*, 704, L118
- Ryder S. D., Murrowood C. E., Stathakis R. A., 2006, *MNRAS*, 369, L32
- Sagar R., Kumar B., Omar A., Joshi C., 2012, in *Astronomical Society of India Conference Series*, vol. 4 of *Astronomical Society of India Conference Series*, 113 – 120
- Sagar R., Omar A., Kumar B., et al., 2011, *Current Science*, 101, 8
- Sanders N. E., Soderberg A. M., Levesque E. M., et al., 2012, *ApJ*, 758, 132
- Schlegel D. J., Finkbeiner D. P., Davis M., 1998, *ApJ*, 500, 525
- Schmidt B. P., Kirshner R. P., Eastman R. G., et al., 1993, *Nature*, 364, 600
- Shigeyama T., Suzuki T., Kumagai S., Nomoto K., Saio H., Yamaoka H., 1994, *ApJ*, 420, 341
- Skillman E. D., Kennicutt R. C., Hodge P. W., 1989, *ApJ*, 347, 875
- Smartt S. J., 2009, *ARA&A*, 47, 63
- Soderberg A. M., Chevalier R. A., Kulkarni S. R., Frail D. A., 2006, *ApJ*, 651, 1005
- Soderberg A. M., Margutti R., Zauderer B. A., et al., 2012, *ApJ*, 752, 78
- Sonbas E., Moskvitin A. S., Fatkhullin T. A., et al., 2008, *Astrophysical Bulletin*, 63, 228
- Stetson P. B., 1987, *PASP*, 99, 191
- Stetson P. B., 1992, in *Astronomical Data Analysis Software and Systems I*, edited by D. M. Worrall, C. Biemesderfer, J. Barnes, vol. 25 of *Astronomical Society of the Pacific Conference Series*, 297
- Stoll R., Prieto J. L., Stanek K. Z., Pogge R. W., 2012, *ArXiv e-prints*, arXiv:1205.2338 [astro-ph.CO]
- Stritzinger M., 2010, *Central Bureau Electronic Telegrams*, 2158, 1
- Stritzinger M., Mazzali P., Phillips M. M., et al., 2009, *ApJ*, 696, 713
- Taubenberger S., Navasardyan H., Maurer J. I., et al., 2011, *MNRAS*, 413, 2140
- Tomasella L., Valenti S., Ochner P., Benetti S., Cappellaro E., Pastorello A., 2011, *Central Bureau Electronic Telegrams*, 2827, 2
- Tremonti C. A., Heckman T. M., Kauffmann G., et al., 2004, *ApJ*, 613, 898
- Van Dyk S. D., Li W., Cenko S. B., et al., 2011, *ApJ*, 741, L28
- Vinkó J., Takáts K., Szalai T., et al., 2012, *A&A*, 540, A93
- Waxman E., Mészáros P., Campana S., 2007, *ApJ*, 667, 351
- Wheeler J. C., Barker E., Benjamin R., et al., 1993, *ApJ*, 417, L71
- Woosley S., Janka T., 2005, *Nature Physics*, 1, 147
- Woosley S. E., Eastman R. G., Weaver T. A., Pinto P. A., 1994, *ApJ*, 429, 300
- Woosley S. E., Pinto P. A., Martin P. G., Weaver T. A., 1987, *ApJ*, 318, 664
- Young T. R., Baron E., Branch D., 1995, *ApJ*, 449, L51